Indian Journal of Geo Marine Sciences
Vol. 53 (03), March 2024, pp. 95-108
DOI: 10.56042/ijms.v53i03.6498

Impact of changing climate on wind power potential at proposed Indian offshore sites using quantile mapping

A S Wadalkar*[a,b] & M C Deo[a]

[a]Department of Civil Engineering, Indian Institute of Technology Bombay, Mumbai, Maharashtra – 400 076, India

[b]Indian National Centre for Ocean Information Services, Hyderabad, Telangana – 500 090, India (Present address)

*[E-mail: as.wadalkar-p@incois.gov.in; aswadalkar10647@gmail.com]

Received 1 November 2023; revised 17 February 2024

Energy extraction from offshore wind is of high priority in India due to the vigorous efforts of the government to replace fossil fuels with renewable ones. There is, however concern about the future sustainability of such power projects against the backdrop of climate change. It is therefore necessary to assess likely changes in the wind potential of identified Indian coastal areas. While previous studies do exist, an update is needed given the availability of more advanced General Circulation Models (GCMs), reanalysis wind data, and LiDAR (Light Detection And Ranging)-based wind speed measurements. This study, therefore, aims to understand future changes in the monthly wind potential at identified offshore sites off the coasts of Gujarat and Tamil Nadu based on the latest GCM suite of models from the Climate Model Inter-comparison Project (CMIP) as well as a high-resolution reanalysis wind data. It compares the results obtained from the CMIP6 suite of models with those from earlier CMIP5 models across three time slices representing the past (1989-2005), near future (2017-2033), and far future (2034-2050) conditions. The seasonal and spatial variations of wind power are explored. The multi-model ensemble median of CMIP6 GCMs, which demonstrates greater agreement with in-situ winds than that of CMIP5, suggests an increase in wind power density during the monsoon season and a decrease in winter at Gujarat. However, at Tamil Nadu, it shows a declining trend from 2017-2050, though winter densities are expected to exceed historical values.

[**Keywords**: Bias correction, Climate change, GCM ensemble, General circulation models, Quantile mapping, Wind potential]

Introduction

Wind energy is an intensively growing renewable energy source in India. Having recently established several land-based wind farms, the Government of India is now looking forward to large-scale extraction of offshore wind energy. Considering this, certain offshore zones off the coasts of Gujarat and Tamil Nadu states have been identified for potential energy extraction[1]. The first offshore wind farm project was initiated in the year 2014. There is, however, a concern about the sustainability of such wind farms, considering the climate change induced by global warming. The likely impact of climate change on India's offshore wind potential thus needs careful consideration[2].

Projected wind information is required to study the changes in future wind power potential, and for this purpose, datasets from Coupled Model Intercomparison projects are popularly used. The initial models, Coupled Model Intercomparison Project-5 (CMIP5) models, were introduced in 2013 in the Inter-Governmental Panel on Climate Change (IPCC)'s 5th assessment report. The individual models under the CMIP5 umbrella were run using the global warming and societal response scenarios called Representative Concentration Pathways (RCPs). In IPCC's 6th assessment report, new and more sophisticated CMIP6 models were introduced as they involve better modelling, computing base and realistic socio-economic pathways. Further in those models, the RCPs have been replaced by Shared Socio-economic Pathways (SSPs). CMIP6 attempts to address the response of the entire earth system to the model forcing by addressing model bias, warming scenario uncertainties and internal model variability, among other features. The SSPs are associated with a forcing ranging from 1.9 to 8.5 W/m^2 and accounting for all socio-economic factors, including gross domestic products, population and poverty levels, to name a few. There are around 21 CMIP6-Endorsed Model Inter-comparison Projects. Some past studies suggest better performance of CMIP6 GCM-based

outcomes over those of CMIP5 GCM-based one. Kamruzzaman *et al*.[3] reported improvement in the CMIP6 ensemble mean over the CMIP5 ensemble mean while assessing rainfall and temperature in Bangladesh. On the other hand, Bourdeau-Goulet & Hassanzadeh[4] showed that CMIP6 and CMIP5 ensemble means are similar, and CMIP6 models do not necessarily outperform CMIP5 models while checking climate variables influencing environmental conditions and socio-economic growth in Canada. Li *et al*.[5], too, found no overall advantage of CMIP6 models over CMIP5 models when studied for total precipitation over the entire globe.

In India, Ministry of New and Renewable Energy (MNRE) acts as a nodal ministry to develop offshore wind energy, and the National Institute of Wind Energy (NIWE), Chennai, serves as a nodal agency for the same. They have identified five zones, named A, B, D, E, and F, off the coast of Gujarat (Fig. 1b) and five zones off the coast of Tamil Nadu (earlier eight zones, zones G, F and H excluded by Ministry of Defense) (Fig. 1c) for this purpose[6-10]. According to the First Offshore Wind Project of India (FOWPI)[11], the first offshore wind farm with a capacity of 1 GW is being set up in the Gujarat zone B, where some in-situ LiDAR-based wind measurements were made at the location of 20°45’19.10” N and 71°41’10.93” E.

There are a few past works in which likely changes in India’s offshore wind climate and wind potential in general, and not necessarily at the above-identified offshore zones, have been assessed. Jaswal & Koppar[12] reported a decreasing trend over the historical period of 1961 to 2008 in near surface winds in India; Shanas & Kumar[13] found a decreasing trend in surface wind speeds at a single location off Goa along the west coast of India; and Kulkarni *et al*.[14,15] used CMIP5 models-based projections, subsequently found substantial rise on the contrary in the monthly wind potentials off Gujarat and Tamil Nadu offshore. Additionally, Karnauskas *et al*.[16] noticed a decrease in wind power potential in the

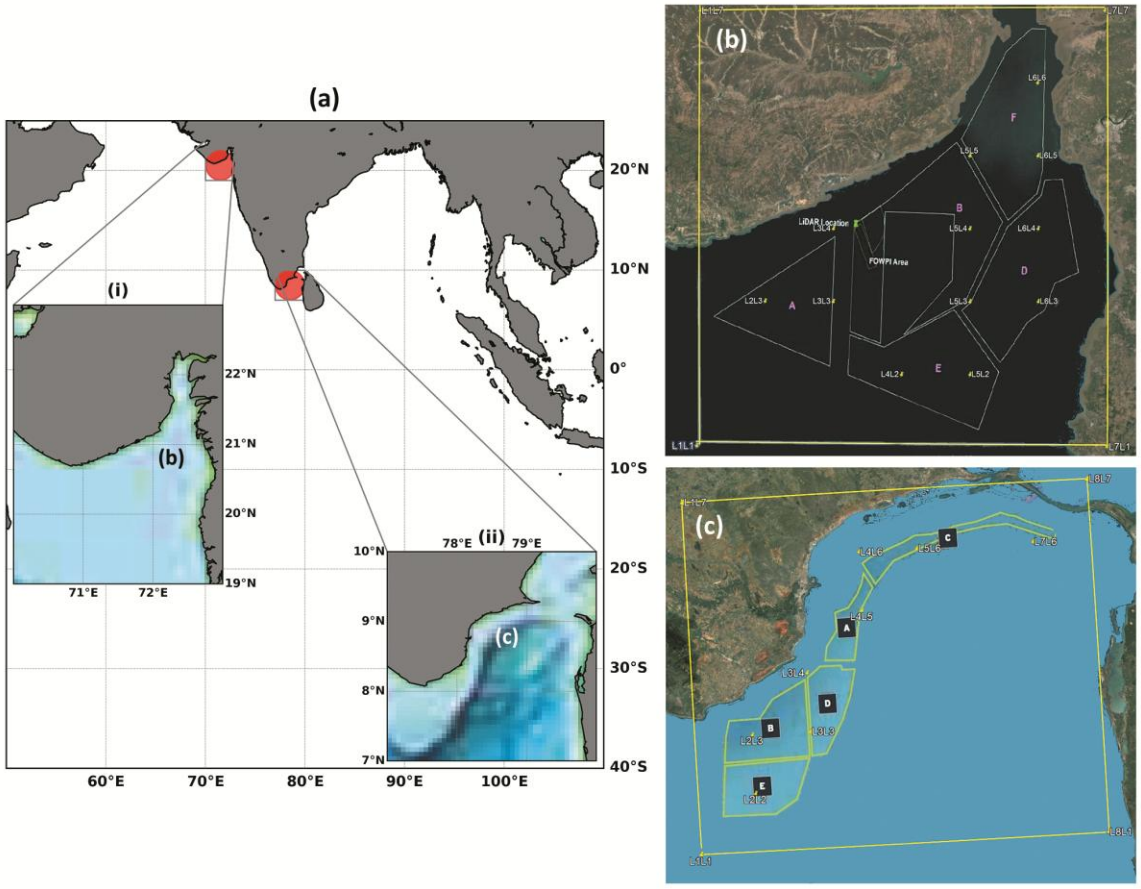

Fig. 1 — (a) Map showing the study regions where offshore wind farms are proposed; (b) Five identified zones in Gujarat with boundaries and allocated grid points; and (c) Five identified zones in Tamil Nadu with boundaries and allocated grid points, obtained by overlaying modified images from NIWE reports(refs. 7 and 11) in Google Earth pro

northern hemisphere and an increase in the subtropical region. Gao *et al*.[17] observed a gradual decrease in wind power potential because of the warming of the Indian Ocean. Lakku & Behera[18] found an increasing trend in the wind speeds in the Indian offshore region from 1979 to 2005 and a decreasing trend from 2006 to 2014.

All the above-mentioned studies were made either at general locations or over a historical time slice and over spatially averaged regions, primarily based on earlier CMIP5 models. With the availability of advanced CMIP6 GCMs, employing them and updating the earlier works has become necessary. Along with these climate models, the recent high-resolution reanalysis of wind information together with available in-situ LiDAR-based wind data[19,20], needs to be used for this purpose.

The aim of this study is, therefore, to understand future changes in monthly wind power potential at identified offshore sites off the coasts of two states of India, namely, Gujarat and Tamil Nadu, based on the latest CMIP6 GCMs as well as on high-resolution reanalysis wind data and in-situ LiDAR-based wind speed measurements. The results obtained from the CMIP6 suite of the models are further compared in this study with those from the earlier CMIP5 models. The seasonal and spatial variations of the wind power in the identified areas are also studied in the three-time slices representing the past (1989-2005), near future (2017-2033) and far future (2034-2050).

Materials and Methods

Study area and data

This study considers eleven individual GCMs, each from the CMIP5 and the CMIP6 umbrella, that have a common origin (Table S1). The selection of GCMs and intercomparison of CMIP5 versus CMIP6 version is made following Kamruzzaman *et al*.[3], Bourdeau-Goulet & Hassanzadeh[4], Li *et al*.[5]; and Kulkarni *et al*.[21]. The moderate or middle-of-the-path RCP 4.5 and SSP 2-4.5 scenarios are selected. The 'r1i1p1' and 'r1i1p1f1' ensemble realizations from CMIP5 and CMIP6 suites, respectively, were chosen for the current study, for a fair comparison of historical and projections scenarios. The eastward (u) and northward (v) surface wind velocities with a temporal resolution of 1 day are used. These belonged to three-time slices of 17 years, namely, past (1989-2005), near future (2017-2033), and far future (2034-2050). The reference reanalysis datasets pertain to the National Oceanic and Atmospheric Administration's (NOAA) National Center for Environmental Prediction (NCEP) Climate Forecast System Reanalysis (CFSR) winds with a resolution of 0.3125° latitude (Lat.) × 0.3125° longitude (Long.) from the years 1989 to 2019. These NCEP-CFSR datasets (hereafter referred as CFSR) are chosen following their accuracy with in-situ measurements[14,15]. In addition, in-situ LiDAR-based wind speeds at 100 m hub height measured at the LiDAR location in Gujarat zone B (Fig. 1b) available from November 2017 to November 2019 are considered to check their closeness with the GCM data, although over a limited period.

The images of identified zones imported from NIWE reports[7-11] are overlayed in Google Earth Pro for georeferencing. Based on the spatial resolution of NCEP-CFSR data and the boundaries of georeferenced zones, the boundary was set from 70.9375° E to 72.8125° E (Lat.) and from 19.827° N to 21.70° N (Long.) for the Gujarat zones (Fig. 1b). The same procedure is followed for the Tamil Nadu region, where the boundaries are set between 77.5° E and 79.6875° E (Long.) and from 7.337° N and 9.212° N (Lat.) (Fig. 1c). For Gujarat, 49 grid points (7 Lat. and 7 Long.) and for Tamil Nadu, 56 grid points (7 Lat. and 8 Long.) are obtained in the set boundary. These grid points are spaced as per the higher resolution of 0.3125° Lat. × 0.3125° Long. of the CFSR wind. The grid points are allocated to different zones as per their coordinates and positions on the georeferenced map of identified zones. The nomenclature of grid points like L3L4, as shown in Figs. 1(b) and 1(c), is done such that they represent the points in a coordinate system formed by boundaries in which the first L represents longitude and the second L represents latitude. The zones of different shapes were identified considering their potential for commercial development, which includes suitable water depths, proximity to ports and oil platforms, pipelines, shipping routes, seismic and cyclone risks, as well as environmental factors such as mangroves and coral reefs[8,9]. The grid points are also allotted as per the size, shape, and location of different zones in CFSR data. The distribution of the grid points is non-uniform since each zone has a different shape.

Evaluation of wind power

To downscale the low-resolution GCM wind to the local and high-resolution level, the technique of bilinear interpolation accompanied by the bias

correction by quantile mapping technique, commonly known as the 'BIQM' technique, is used, as done earlier in Dragini *et al*.[22], Li *et al*.[23] and Kulkarni *et al*.[14,21]. Accordingly, the cumulative distribution functions of the given GCM-based wind and standard CFSR wind are matched in their quantiles. The GCM-based wind was replaced directly by CFSR wind for the historical data, while for the projected wind, the difference between the future GCM and past GCM wind is added to the CFSR wind at a given probability level as done earlier in Kulkarni *et al*.[14,21]. This methodology is adopted as it is widely used in downscaling, and Kulkarni *et al*.[14] found it superior to ANN-based downscaling.

The northward and eastward wind speeds, u and v, respectively, at the hub height of 100 m, are obtained from their given values at 10 m height using the 1/7th power law. The resultant wind speed, U_R, is derived thereafter using eq. (1) as stated below[14,21]:

$$U_R = \sqrt{u^2 + v^2} \quad \ldots (1)$$

Such wind speeds are fitted to the Weibull distribution, following Kulkarni *et al*.[14,21], and the wind power potential or power density is derived using eq. (2) as in Al-Buhairi & Al-Haydari[24]:

$$\frac{\bar{P}}{A} = \frac{1}{2}\rho c^3 \Gamma\left(1 + \frac{3}{k}\right) \quad \ldots (2)$$

In the above equation, P = power density, A = swept area of the turbine blades, ρ = air density, c = Weibull scale parameter, $\Gamma(.)$ = Gamma function, and k = Weibull shape parameter.

For seasonal analysis, the wind speeds are grouped into three main seasons: monsoon (June to September), winter (October to February) and summer (March to May). Further, following Akpinar & Akpinar[25] and Kulkarni *et al*.[15], two characteristic wind speeds, namely, the most probable speed, V_{mp}, and the maximum speed V_{max} are calculated from the Weibull fits using eqs. (3) and (4):

$$V_{mp} = c\left(\frac{k-1}{k}\right)^{\frac{1}{k}} \quad \ldots (3)$$

$$V_{max} = c\left(\frac{k+2}{k}\right)^{\frac{1}{k}} \quad \ldots (4)$$

For Gujarat zones, after noticing an increase in the difference between GCM winds and LiDAR after bias correction, the LiDAR correction was added which is the mean difference between bias-corrected GCM wind speed and in-situ LiDAR speed. The LiDAR correction for the Multi-Model Ensemble (MME) of CMIP5 is 2.66 m/s for winter, 3.31 m/s for summer, and 2.75 m/s for monsoon. These values for MME of CMIP6 are 2.76 m/s for winter, 3.48 m/s for summer, and 2.61 m/s for monsoon. Such LiDAR-based correction is made considering that the wind power density is a cubic function of wind speed.

Mann Kendall's non-parametric test[26-28] is employed to check the trend of obtained wind power densities based on corrected wind and raw downscaled winds. The Kendall Tau-b coefficient is similarly used to assess the association between CMIP5 and CMIP6-based power densities, as done by Kulkarni *et al*.[14,15].

Results

The association between the historical GCM and the standard CFSR reanalysis wind speeds are studied in the beginning, as given below.

Comparison of GCM and CFSR winds

The variation of the past wind speed and bias across the GCM and CFSR winds for Gujarat zones are shown for one example case of the ACCESS 1-0 model in Figures 2(a) and 2(b), respectively. Such comparisons across the historical wind speeds of GCM and CFSR indicated that for most of the GCMs, the difference between them reduced after the removal of the bias. These figures pertained to raw or uncorrected data, while Figures 2(c) and 2(d) show the same for the bias-adjusted data. It is noticed that when all GCMs are viewed together, the bias in the wind of the historical period (1989-2005) varied from -5 m/s to 5 m/s before the correction and from -0.1 m/s to 0.1 m/s after the bias removal.

The difference between the wind speeds of every individual GCM model (within the umbrella of both CMIP5 and CMIP6) and corresponding CFSR wind speeds is studied to derive the error statistics of the correlation coefficient, R, Mean Absolute Error (*MAE*) and Root Mean Square Error (*RMSE*). While R represents the degree of linear association between them, the *MAE* indicates the error that is not biased towards the high values. The *RMSE*, on the other hand, provides a good measure of the high-value effects. Table 1 shows the same for Gujarat as well as Tamil Nadu zones. For each GCM, the first row belongs to the CMIP5 suite, while the second pertains to the CMIP6 suite. The last row indicates the MME cases of CMIP5 and CMIP6. The more correlated version among CMIP5 and CMIP6 has been

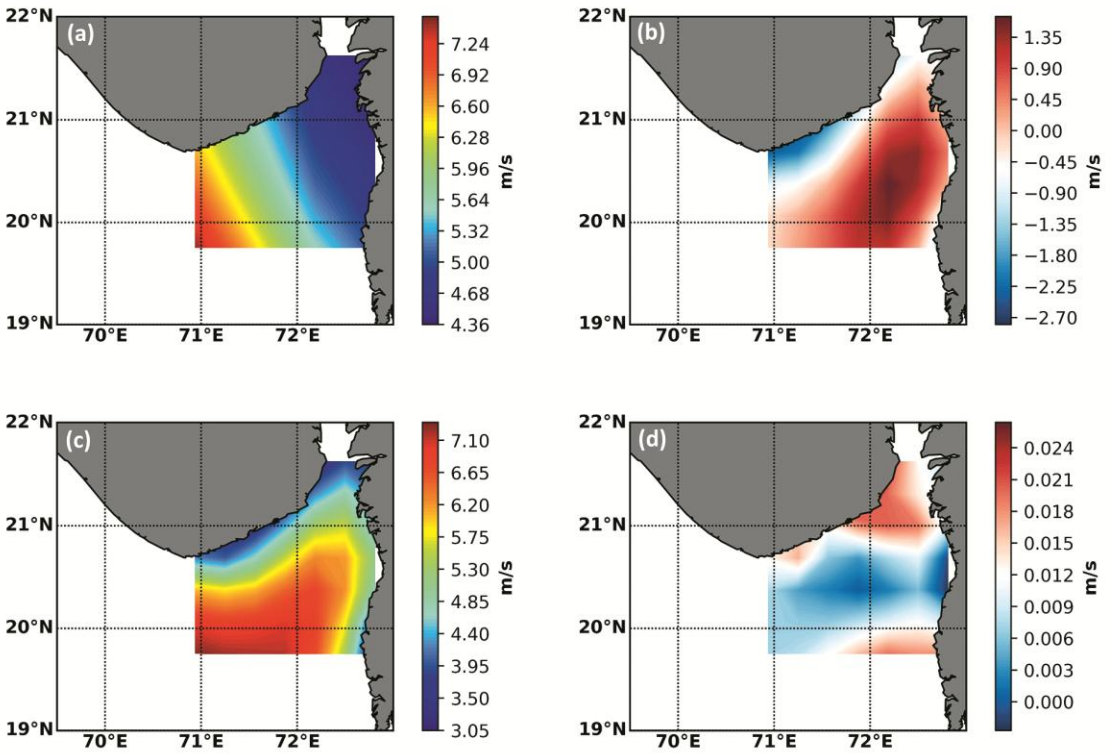

Fig. 2 — (a) Wind speed variation of raw downscaled ACCESS1-0 GCM; (b) Bias of raw downscaled model simulated speed with CFSR simulated winds (broad range); (c) Wind speed variation of bias corrected GCM simulated winds; and (d) Bias of corrected winds with CFSR simulated winds (narrow range) over historical time slice in Gujarat

Table 1 — Association between GCM and CFSR simulated wind speeds over the past period

Datasets	Gujrat (49 grid points)			Tamil Nadu (56 grid points)		
	R (Corr. Coeff)	*MAE* (m/s)	*RMSE* (m/s)	*R* (Corr. Coeff)	*MAE* (m/s)	*RMSE* (m/s)
CFSR and ACCESS-10	**0.9061**	0.9020	1.1583	**0.8411**	1.6150	2.139
CFSR and ACCESS-CM2	0.8601	1.0942	1.3884	0.8336	1.7190	2.1801
CFSR and ACCESS-1-3	0.8617	1.0734	1.3897	**0.8111**	1.7017	2.3076
CFSR and ACCESS-ESM-1-5	**0.8987**	0.9388	1.2009	0.7996	1.8511	2.3695
CFSR and BCC-CSM-1.1m	0.8503	1.1751	1.483	0.7697	1.9410	2.5237
CFSR and BCC-CSM2-MR	**0.8600**	1.1250	1.4254	**0.8026**	1.8598	2.3767
CFSR and CanESM2	**0.8952**	0.9424	1.2199	0.8502	1.6076	2.0771
CFSR and CanESM5	0.8944	0.9615	1.2286	**0.8716**	1.4680	1.9376
CFSR and GFDL-CM3	0.8137	1.2648	1.5886	0.6799	2.2909	2.9437
CFSR and GFDL-CM4	**0.8933**	0.9670	1.2377	**0.7750**	1.9051	2.4944
CFSR and GFDL- ESM2G	0.8759	1.0286	1.3229	**0.8072**	1.8055	2.3287
CFSR and GFDL- ESM4	**0.8913**	0.9612	1.2506	0.7204	2.1130	2.7476
CFSR and INMCM4	0.7280	1.4476	1.8772	0.4224	3.2157	3.9245
CFSR and INM-CM4-8	**0.9187**	0.8618	1.097	**0.7910**	1.8747	2.414
CFSR and IPSL-CM5A-LR	**0.8983**	0.9497	1.214	**0.8017**	1.7944	2.3659
CFSR and IPSL-CM6A-LR	0.8118	1.2508	1.5962	0.8007	1.8623	2.3639
CFSR and MIROC5	**0.9075**	0.8863	1.1476	0.7734	1.9566	2.5007
CFSR and MIROC6	0.8840	0.9758	1.2772	**0.7934**	1.9097	2.4014

(*Contd*.)

Table 1 — Association between GCM and CFSR simulated wind speeds over the past period (*Contd*.)

	Gujrat (49 grid points)			Tamil Nadu (56 grid points)		
	R (Corr. Coeff)	*MAE* (m/s)	*RMSE* (m/s)	*R* (Corr. Coeff)	*MAE* (m/s)	*RMSE* (m/s)
CFSR and MPI-ESM-LR	**0.9013**	0.9377	1.1913	0.8170	1.8439	2.2876
CFSR and MPI-ESM-1-2-LR	0.8954	0.9442	1.2219	**0.8225**	1.7444	2.2439
CFSR and MRI-CGCM3	0.8358	1.1619	1.5047	**0.7528**	2.0001	2.6026
CFSR & MRI-ESM-2.0	**0.8781**	1.0329	1.3217	0.7368	2.0862	2.6819
CFSR & MME-CMIP5	0.9220	0.8834	1.1301	0.8564	1.6176	2.0963
CFSR & MME-CMIP6	**0.9306**	0.8310	1.0622	**0.8680**	1.5807	2.0211

highlighted in bold in Table 1. (The same description is valid for Table 2, referred to subsequently).

Table 1 show that the association between a given individual GCM does not depend on the region (Gujarat or Tamil Nadu), the model suite (CMIP5 or CMIP6) or any individual GCM within them. However, regarding MME, the CMIP6 MME is more associated with the CFSR wind than the CMIP5 MME for both Gujarat and Tamil Nadu.

Analysis at LiDAR location in Gujarat

As the in-situ measurements by LiDAR are available over a two-year period ranging from Nov. 2017 to Nov. 2019, these monthly mean wind speeds at 100 m hub height are compared with corresponding ones of GCM and CFSR at the LiDAR location to know the association between these sets of wind data. Table 2 shows the same with respect to GCM and LiDAR as well as GCM and CFSR data in two separate cases of BIQM-based bias-corrected wind and bias-uncorrected wind.

The MME wind speed of CMIP6 shows a slightly better correlation with CFSR wind than the MME wind of CMIP5. Generally, a particular GCM under either CMIP5 or CMIP6 that had a good correlation with CFSR wind also indicated a fair resemblance with in-situ LiDAR data. It is further noticed that the difference between GCM and LiDAR wind increased after bias correction (Fig. 3a, 3b & Table 2). Further, the MME of bias-uncorrected CMIP6 GCMs has the highest correlation with in-situ LiDAR data, and this is followed by individual INM-CM4-8, MPI-ESM-LR, and then the MME of CMIP5 GCMs. The models with more than a 0.9 correlation coefficient with in-situ data are highlighted in this Table in bold. Similar observations are made while further assessing the closeness of GCM and CFSR wind, as in Table 2.

The differences across MME-CMIP5, MME-CMIP6, CFSR, and LiDAR monthly wind speeds over the two years of LiDAR measurement period are graphically shown in Figure 3(a) for the bias-uncorrected (R-CMIP6 and R-CMIP5) and in Figure 3(b) for the bias-corrected (B-CMIP6 and B-CMIP5) wind data. Figure 3(b) also shows LiDAR-corrected (L-CMIP6 and L-CMIP5) winds in which the MMEs of GCMs are corrected by adding the mean absolute error (with respect to LiDAR) seasonally and used further for the prediction of future offshore wind potential densities. It is observed that after adding LiDAR corrections, the *R*-value between LiDAR (and bias) corrected MME of CMIP5 GCMs with LiDAR data is 0.93 and *MAE* is 0.47 m/s. The exact values for CMIP6 data were 0.94 and 0.45, respectively. It may be noted that the correlation coefficient between LiDAR and CFSR winds is 0.9000 while the *MAE* is about 1.9784 m/s and *RMSE* is about 2.3471 m/s, which suggests a relatively weaker match than some of the CMIP5 and CMIP6 GCM based winds as well as the ensemble median of them. The possible reasons are discussed in the discussion section.

Changes in wind potential – Gujarat and Tamil Nadu zones

The resulting CMIP5 and CMIP6-based monthly wind potentials over the three-time slices, and the corresponding percentage change in the future potential from the historical period for a typical case of Gujarat zone A is shown in Figure 4. It may be seen from Figures 4(c) and 4(d) that the magnitude of the changes would be relatively higher over the winter months (Oct – Mar) than the summer or monsoon months, although overall, these are generally small. The season-wise variations for both CMIP5 and CMIP6 cases in the most probable wind velocity, V_{mp}, the maximum velocity, V_{max}, and wind power density, *WPD*, over the three-time slices (past, near-future, and far-future) as per the seasons are shown in Table 3, which pertain to Gujarat zone A, located towards the open Arabian Sea and F situated landwards, respectively.

From Table 4, it is apparent that at zone ‘A’, in the monsoon season, both CMIP5 and CMIP6-based characteristic wind speeds and power densities would

Table 2 — Closeness of GCM simulated speeds, in-situ LiDAR wind speeds and CFSR wind speeds (2017-2019)

Datasets	Bias corrected (BIQM) GCM			Raw downscaled (BI) GCM		
	R (Corr. Coeff)	*MAE* (m/s)	*RMSE* (m/s)	*R* (Corr. Coeff)	*MAE* (m/s)	*RMSE* (m/s)
LiDAR and ACCESS-10	**0.9040**	2.9851	3.017	**0.9063**	1.9361	2.0951
LiDAR and ACCESS-CM2	0.8568	3.0250	3.0843	0.8567	2.8742	2.9695
LiDAR and ACCESS-1-3	0.8386	2.8526	2.9099	0.8469	2.1881	2.2748
LiDAR and ACCESS-ESM-1-5	0.8680	2.9313	2.9576	0.8726	2.5794	2.609
LiDAR and BCC-CSM-1.1m	0.8321	2.9525	2.9832	0.8295	1.6570	1.8237
LiDAR and BCC-CSM2-MR	0.8715	2.8709	2.883	0.8775	1.3272	1.4364
LiDAR and CanESM2	0.8608	2.8889	2.9245	0.8614	1.033	1.2235
LiDAR and CanESM5	0.8495	3.2734	3.2999	0.8528	1.5877	1.7144
LiDAR and GFDL-CM3	0.7968	3.1352	3.1749	0.7944	3.1958	3.2295
LiDAR and GFDL-CM4	0.8758	2.9699	2.9746	0.8774	1.2796	1.4897
LiDAR and GFDL- ESM2G	0.77	2.9125	2.998	0.7697	1.6818	1.8698
LiDAR and GFDL- ESM4	0.8765	2.9033	2.9223	0.8815	1.2382	1.3951
LiDAR and INMCM4	0.3663	3.1521	3.3817	0.3685	2.1707	2.4375
LiDAR and INM-CM4-8	**0.9407**	2.8640	2.8241	**0.9441**	1.4676	1.5468
LiDAR and IPSL-CM5A-LR	0.9255	2.9445	2.8991	0.9233	3.1000	3.0448
LiDAR and IPSL-CM6A-LR	0.7526	2.9369	3.0245	0.7528	1.6355	1.8517
LiDAR and MIROC5	0.7947	2.7559	2.8822	0.7950	1.5667	1.9147
LiDAR and MIROC6	0.8802	3.0044	3.0044	0.8809	2.2622	2.7183
LiDAR and MPI-ESM-LR	**0.9370**	2.9823	2.9388	**0.9370**	1.6933	1.7926
LiDAR and MPI-ESM-1-2-LR	0.8626	3.1234	3.1126	0.8636	1.4147	1.6013
LiDAR and MRI-CGCM3	0.8878	3.0369	3.0122	**0.9041**	**0.6793**	0.8665
LiDAR and MRI-ESM-2.0	0.7895	2.9683	3.0278	0.7972	1.1885	1.5563
LiDAR and MME-CMIP5	**0.9147**	2.9646	2.9758	**0.9153**	1.7175	1.781
LiDAR and MME-CMIP6	**0.9375**	3.0049	2.9474	**0.9553**	1.4448	1.487
CFSR and ACCESS-10	**0.8971**	1.6112	1.8885	**0.8968**	1.2481	1.4183
CFSR and ACCESS-CM2	**0.8484**	1.8351	2.0926	**0.8488**	1.7169	1.9844
CFSR and ACCESS-1-3	**0.8878**	1.8236	1.9626	**0.8858**	1.7088	1.9419
CFSR and ACCESS-ESM-1-5	**0.8647**	1.8278	2.0502	**0.8656**	1.7546	1.9734
CFSR and BCC-CSM-1.1m	**0.7670**	2.1514	2.3771	**0.7485**	1.8889	2.0977
CFSR and BCC-CSM2-MR	**0.7824**	2.0786	2.2652	**0.7763**	1.6238	2.0114
CFSR and CanESM2	**0.7826**	1.9578	2.241	**0.7765**	2.0910	2.495
CFSR and CanESM5	**0.8371**	2.0565	2.2982	**0.8286**	1.5469	1.7593
CFSR and GFDL-CM3	**0.7194**	2.2769	2.5715	**0.7115**	2.3898	2.721
CFSR and GFDL-CM4	**0.9053**	1.7340	2.0031	**0.9053**	1.3157	1.5278
CFSR and GFDL- ESM2G	**0.7416**	2.0124	2.3637	**0.7358**	1.8502	2.1749
CFSR and GFDL- ESM4	**0.8583**	1.8166	2.0547	**0.8600**	1.6002	1.8684
CFSR and INMCM4	**0.4916**	2.5725	2.8645	**0.4947**	2.2118	2.6644
CFSR and INM-CM4-8	**0.9056**	1.6186	1.8811	**0.9001**	1.3805	1.5504
CFSR and IPSL-CM5A-LR	**0.8703**	1.8148	2.1016	**0.8653**	1.9897	2.3382
CFSR and IPSL-CM6A-LR	**0.6815**	2.1679	2.5648	**0.6791**	1.9407	2.2718
CFSR and MIROC5	**0.7978**	1.7599	2.1288	**0.7980**	1.6520	1.9044
CFSR and MIROC6	**0.8007**	1.9498	2.2703	**0.8026**	1.7428	2.0547
CFSR and MPI-ESM-LR	**0.8437**	1.8854	2.1202	**0.8387**	1.5130	1.6989
CFSR and MPI-ESM-1-2-LR	**0.7602**	1.9399	2.4922	**0.7610**	1.7723	2.0092
CFSR and MRI-CGCM3	**0.8753**	1.9102	2.2224	**0.8815**	2.2150	2.4964
CFSR and MRI-ESM-2.0	**0.8292**	1.9710	2.2417	**0.8333**	2.3997	2.7984
CFSR and MME-CMIP5	**0.8757**	1.9203	2.1252	**0.8800**	1.5343	1.7392
CFSR and MME-CMIP6	**0.9036**	1.8588	2.1055	**0.9171**	1.3649	1.5453

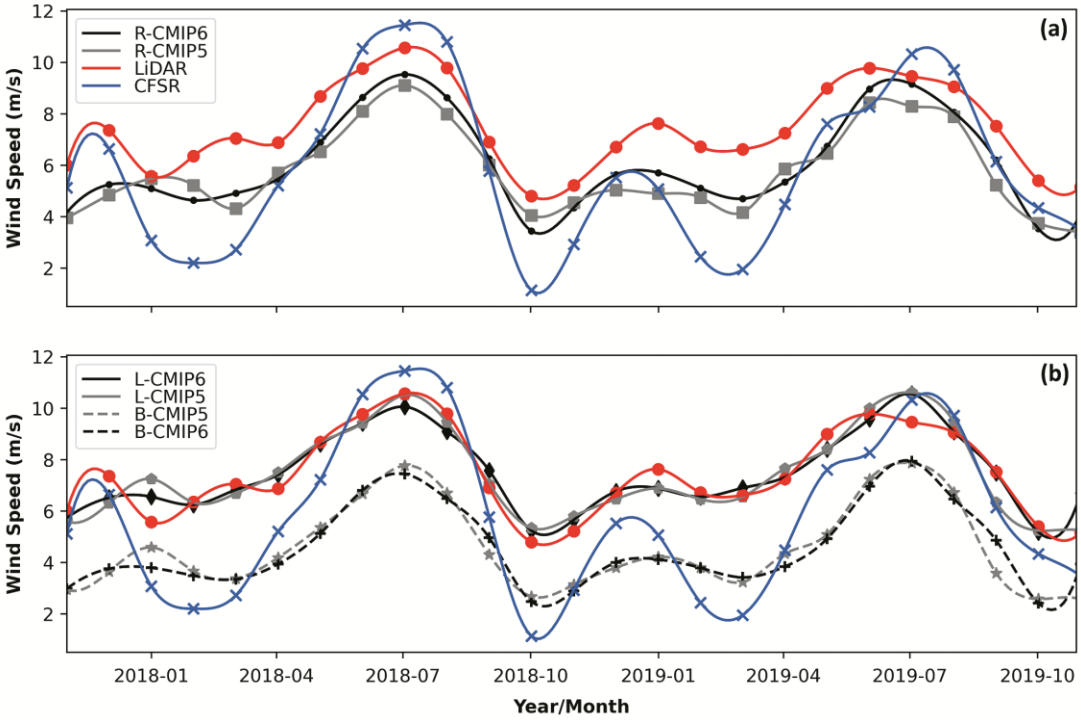

Fig. 3 — (a) Comparison between wind speeds from in-situ LiDAR measurements (Lidar), CFSR (CFSR), raw downscaled MMEs of CMIP5 (R-CMIP5) and CMIP6 (R-CMIP6) GCMs at LiDAR location in Gujarat zone B; and (b) Comparison between bias-corrected MMEs of CMIP5 (B-CMIP5) and CMIP6 (B-CMIP6) having difference with LiDAR measured speed, corrected in L-CMIP5 and L-CMIP6 which are used for predictions of *WPD*s

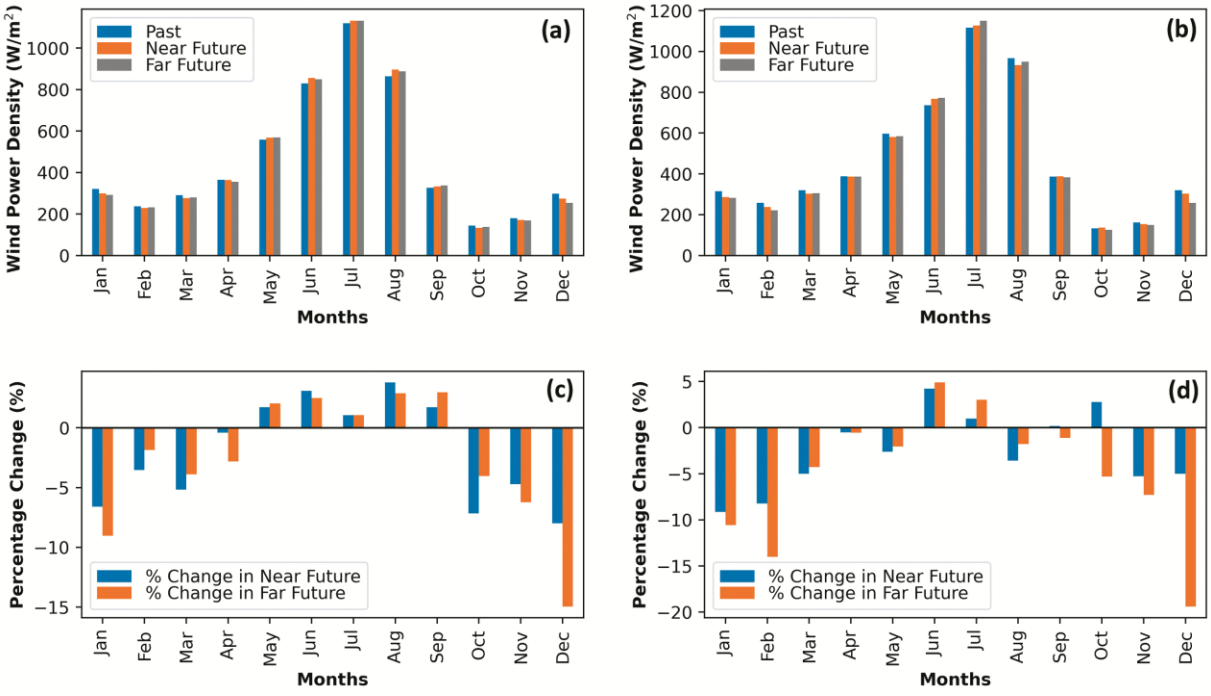

Fig. 4 — Monthly *WPD*s based on (a) CMIP5 MME and (b) CMIP6 MME in considered past and future slices, followed by percentage change in future slices relative to historical slice based on (c) CMIP5 MME and (d) CMIP6 MME in Gujarat Zone A

Table 3 — Seasonal analysis at Gujarat zone A and landward zone F with change in *WPD* where V_{mp} and V_{max} are in (m/s) and *WPD* is in (W/m^2)

G-Zone A	***Past***			***Near future***				***Far future***			
CMIP-5 MME	V_{mp}	V_{max}	*WPD*	V_{mp}	V_{max}	*WPD*	Change (%)	V_{mp}	V_{max}	*WPD*	Change (%)
Monsoon	11.218	11.81	789.762	11.304	11.896	807.801	2.284	11.304	11.875	806.417	2.109
Winter	7.49	7.967	237.67	7.332	7.795	222.854	-6.234	7.288	7.723	218.072	-8.246
Summer	9.032	9.359	407.212	9.011	9.369	405.15	-0.506	8.998	9.377	404.057	-0.775
CMIP-6 MME	V_{mp}	V_{max}	*WPD*	V_{mp}	V_{max}	*WPD*	Change (%)	V_{mp}	V_{max}	*WPD*	Change (%)
Monsoon	11.327	11.853	808.675	11.332	11.863	809.986	0.162	11.381	11.905	820.052	1.407
Winter	7.427	7.921	232.412	7.261	7.723	216.503	-6.845	7.166	7.629	208.339	-10.358
Summer	9.25	9.549	436.958	9.168	9.488	425.552	-2.61	9.184	9.494	427.64	-2.132
G-Zone F	***Past***			***Near future***				***Far future***			
CMIP-5 MME	V_{mp}	V_{max}	*WPD*	V_{mp}	V_{max}	*WPD*	Change (%)	V_{mp}	V_{max}	*WPD*	Change (%)
Monsoon	10.602	11.143	665.644	10.664	11.22	676.012	1.558	10.655	11.198	675.679	1.508
Winter	6.554	6.851	156.513	6.463	6.774	150.406	-3.902	6.431	6.714	147.748	-5.6
Summer	8.687	9.152	367.023	8.71	9.232	372.262	1.428	8.687	9.245	371.039	1.094
CMIP-6 MME	V_{mp}	V_{max}	*WPD*	V_{mp}	V_{max}	*WPD*	Change (%)	V_{mp}	V_{max}	*WPD*	Change (%)
Monsoon	11.327	11.853	808.675	11.332	11.863	809.986	0.162	11.381	11.905	820.052	1.407
Winter	7.427	7.921	232.412	7.261	7.723	216.503	-6.845	7.166	7.629	208.339	-10.358
Summer	9.25	9.549	436.958	9.168	9.488	425.552	-2.61	9.184	9.494	427.64	-2.132

Table 4 — Impact (% Change) in per future slice *WPD* at Gujarat zone A, Gujarat zone F and Tamil Nadu zone A

Gujarat zone A	*Past*	*Near future*		*Far future*	
	WPD (W/m^2)	*WPD* (W/m^2)	Change (%)	*WPD* (W/m^2)	Change (%)
CMIP5 MME	468.349	467.617	-0.156	464.986	-0.718
CMIP6 MME	478.938	470.129	-1.839	470.495	-1.763
Gujarat zone F	*Past*	*Near future*		*Far future*	
	WPD (W/m^2)	*WPD* (W/m^2)	Change (%)	*WPD* (W/m^2)	Change (%)
CMIP5 MME	382.232	384.456	0.582	382.85	0.162
CMIP6 MME	383.097	377.005	-1.59	380.614	-0.648
Tamil Nadu zone A	*Past*	*Near future*		*Far future*	
	WPD (W/m^2)	*WPD* (W/m^2)	Change (%)	*WPD* (W/m^2)	Change (%)
CMIP5 MME	368.448	361.022	-2.0156	351.401	-4.627
CMIP6 MME	365.168	359.424	-1.5723	356.061	-2.494

increase while the same would decrease in the summer and winter. Further, at zone 'F', CMIP5-based wind power densities might increase in summer in the near future as well as in the far future; while CMIP6-based power densities might decrease in the near future and slightly increase in the far future in the summer season. In the monsoon season, both GCM suites indicate an increase, and in the winter, a decrease in the near and far-future slice. When overall GCM wind speeds for the entire time slices are considered, it is observed that at Gujarat zone A, MMEs of both CMIP6 and CMIP5 GCMs predicted a decrease in the near future as well as in the far-future slice (Table 4). At the landward zone F, the MME of CMIP5 GCMs predicts an increase and the MME of CMIP6 GCMs predicts a decrease in both future slices (Table 4). A similar analysis performed for all other zones in Gujarat agrees with this.

The analysis above is repeated for the Tamil Nadu zones. Typical results of the seasonal analysis for zone A are given in Table S2. These indicate that in the far future slice and according to MME of CMIP5, a decrease in characteristic wind speed as well as power density could happen in all seasons, except summer. In contrast, according to the MME of CMIP6 GCMs, an increase in the same in winter and a decrease in summer and monsoon seasons can occur. Similar trends are observed in the rest of the zones off Tamil Nadu.

Trends in projected wind power density

The trend in wind power densities over the future period of 2017 to 2050 is exemplified in the time series plot of Figure 5(a) that pertains to Gujarat zone A based on CMIP6 MME. When Mann-Kendall's trend test at alpha = 0.1 or 90 % confidence is applied, it is found that such a trend is not statistically significant.

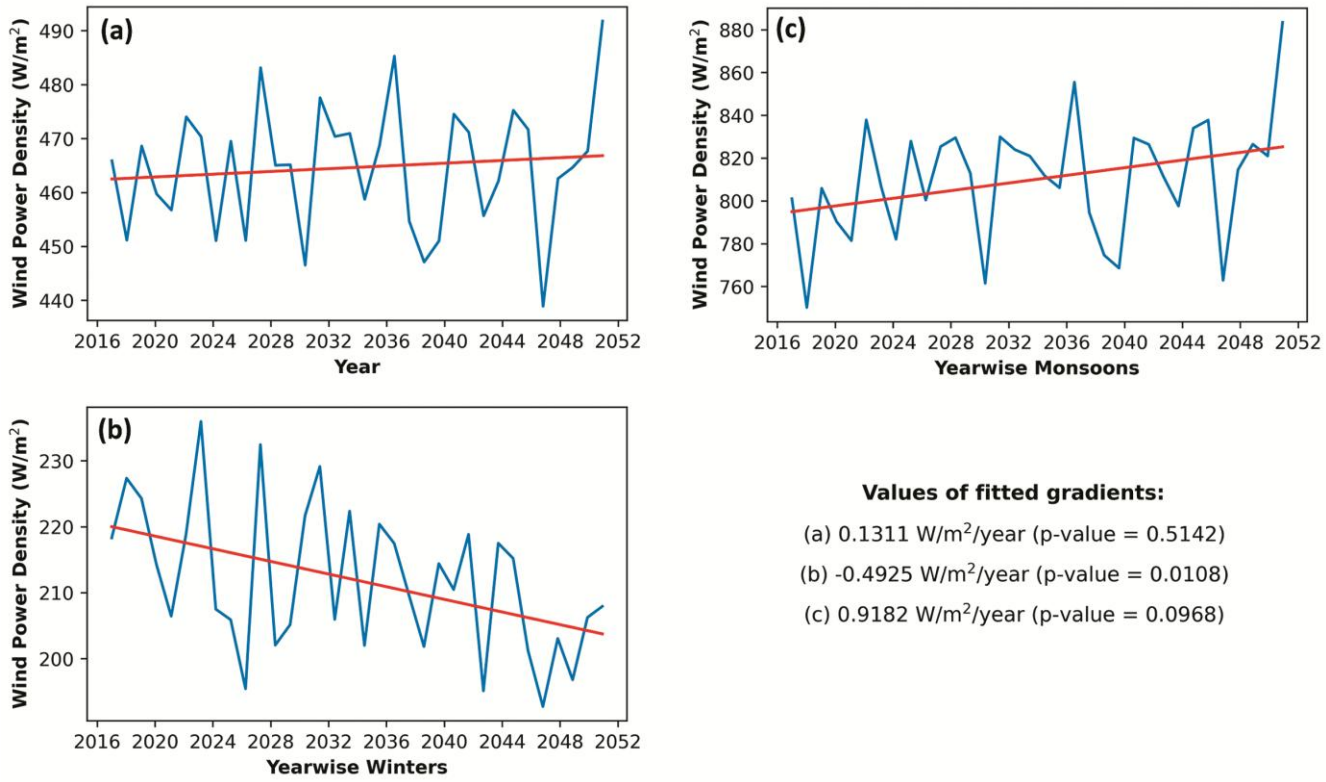

Fig. 5 — (a) CMIP6-MME simulated monthly *WPD*s (all seasons combined averaged annually); (b) CMIP6-MME simulated monthly winter *WPD*s averaged yearly; and (c) CMIP6-MME simulated monthly summer *WPD*s averaged yearly at Gujarat zone A; where trend in (b) and (c) is statistically significant

Further, the slope of the time series is positive with medium confidence (~49 %, p = 0.5142). However, hen seasonal parameters are considered, significantly increasing or decreasing trends (90 % confidence), are seen depending on the season. This can be noticed from the example of the trend of CMIP6-MME wind power density in Figure 5(b), where there is a significant decreasing trend for winter, and in Figure 5(c), where the increasing trend for monsoon at the same Zone A of Gujarat over the years (2017-2050) is shown. The monthly potentials are average over every year to estimate the gradients in W/m^2/year. Table S3 shows all the seasonal trends, and statistically significant trends are highlighted in bold. Table S4 describes the same but for the wind power densities calculated from raw downscaled CMIP winds. Overall, CMIP6-based wind power densities show a statistically significant decreasing trend in the winter season in most of the zones of Gujarat and Tamil Nadu. Further, in the monsoon season, statistically significant increasing trends are observed in all the Gujarat zones when per-year trends are estimated. CMIP5-based wind power densities show a statistically significant decreasing trend for Tamil Nadu zones in monsoon and winter.

Closeness between MME of CMIP5 and CMIP6 simulated winds

In the next part of the study, the closeness of MMEs of CMIP5 and CMIP6 daily winds is noted using Kendall's rank correlation τ_b. This is shown in Table 5 for the three separate times slices of past, near-future, and far-future. As these values are well above the threshold of 0.60, a statistically significant association between these two data sets is confirmed. In addition to τ_b, the association between these two MMEs is also confirmed through the p-value, which is almost zero at 95 % confidence in all the cases indicating the closeness across these two data sets.

Discussion

CMIP6 versus CMIP5 MMEs

As mentioned earlier, the MME wind of CMIP6 is closer to in-situ LiDAR data than that of CMIP5 MME; however, there is no clear superiority when their individual versions are considered, which is in

Table 5 — Kendall's rank correlation coefficient τ_b between CMIP5 and CMIP6 GCM MME-based wind power densities

Gujarat	*Past slice*	*Near future slice*	*Far future slice*	*Combined*
Zone A	0.67665	0.68254	0.69185	0.68443
Zone B	0.69463	0.69605	0.70723	0.69994
Zone D	0.69276	0.69358	0.70649	0.69817
Zone E	0.67776	0.68207	0.69450	0.68552
Zone F	0.70509	0.70317	0.71203	0.70710
Tamil Nadu	*Past slice*	*Near future slice*	*Far future slice*	*Combined*
Zone A	0.64358	0.62795	0.62083	0.63190
Zone B	0.63270	0.62457	0.61175	0.62454
Zone C	0.65917	0.64615	0.64514	0.65056
Zone D	0.63864	0.62638	0.61610	0.62836
Zone E	0.63082	0.62126	0.60497	0.62068
Zone F	0.65868	0.64958	0.64933	0.65266
Zone G	0.63196	0.62496	0.61070	0.62416

line with the findings of Krishnan & Bhaskaran[29] and Kamruzzman *et al*.[3]. The accuracy of GCMs varied from location to location and further, from one season to another.

GCM, CFSR, and LiDAR winds

The analysis of historical GCM, CFSR, and LiDAR data for the two-year duration (2017-2019) shows that the GCMs with a high correlation with CFSR reanalysis data also have so with LiDAR data. The individual GCMs of MRI-CGCM3 (CMIP5) and MRI-ESM-2.0 (CMIP6), MPI-ESM-LR (CMIP5) are more associated with in-situ LiDAR data. In the past, Lakku & Behera[18] and Krishnan & Bhaskaran[29] found GCMs of MPI base to be among the best-performing climate models. In line with model performance study by Kamruzzaman *et al*.[3] in Bangladesh, it has been found that ACCESS1-0 (CMIP5), ACCESS1-3 (CMIP5), CanESM5 (CMIP6), IPSL-CM6A-LR (CMIP6), MIROC6 (CMIP6) are closer to CFSR wind data than their respective counterparts in Tamil Nadu (Table 1). The poor skill of INM-CM4, as observed in Kamruzzaman *et al*.[3] is also confirmed in this work.

The relatively fragile match between LiDAR and CFSR compared to some CMIP-based winds may be arising because the data used in assimilation for CFSR is collected from RAMA (Research Moored Array for African-Asian-Australian Monsoon Analysis and Prediction) observation sites, which are far from our concerned region. The divergence between drifter-measured currents and CFSR-based currents was previously reported by Saha *et al*.[30]. In subsequent versions of CFSR too, stronger variability and higher amplitude of sea-surface temperature was forecasted[31]. In addition, since this study used ensemble median where the median of considered models is estimated at every time stamp, the internal variability among the individual CMIP models is assumed to get cancelled out, bringing the simulations more robust. The new CMIP6 models have been reported for their accuracy in the Indian Ocean; for example, Sajidh & Chatterjee[32] found that CMIP6-based wind circulation-driven dynamic sea level had more fidelity than satellite-based topography products in the tropical Indian Ocean region while checking the mean state and variability. However, the coarser resolution of CMIP models does not allow them to mimic the spatial variations as closely as CFSR, as shown in Figure 2.

The models of BCC-CSM2-MR, CanESM5, MPI-ESM-1-2HR, and IPSL-CM6A-LR were reported to be high-performing CMIP6 GCMs in the Bay of Bengal region by Krishnan & Bhaskaran[29]. Herein, the same pattern is observed in Tamil Nadu. BCC-CSM2-MR performed well over its CMIP5 counterpart in both Gujarat and Tamil Nadu zones.

Bias correction

The positive impact of bias correction was presented by Hagemann *et al*.[33], in their precipitation data analysis for the past time slice of 1961-1990 and the future time slice of 2070-2100 using three GCMs, suggested that it might alter the climate change signal at some locations. In addition, there are some past studies indicating both an increase or decrease in the uncertainty with the bias correction (Themeßl *et al*.[34]; Maraun[35]). Maurer & Pierce[36] analyzed the bias-corrected precipitation ensemble and found that the bias correction could change the trend of the raw GCMs. However, it may not have any adverse effect on the ensemble mean. Cannon *et al*.[37] found that quantile mapping could inflate the trends of raw GCM. The author also argued that the quantile mapping method effectively corrected biases in

historical time, but it corrupts the projected trends over the future raw GCMs. In this study, too, it is noticed that the bias correction by quantile mapping helps to reduce the bias in historical time slices; however, for future predictions, the raw downscaled GCM simulations, rather than the bias-corrected ones, are better correlated with in-situ observations of wind speed. However, some sort of bias correction is necessary for impact studies based on GCM projections[30]. Nevertheless, quantile mapping is a commonly used method, the choice of which is done following its superior performance as stated by Kulkarni *et al*.[15].

In this study, it is found that bias correction does not intensively alter the trends in the projected winds, as described in Tables S3 & S4. The trends in raw downscaled GCM ensemble and bias-corrected trends are almost similar at all the zones, however, with varying confidence (*p*-value). The reason behind this may be that the bias correction has the same effect on each future year. The signs of trends almost remain intact; hence, the effect of bias correction on GCM-based trends is nominal.

The study presented here is limited only to bias correction technique of quantile mapping. Impact analysis using ANN-based downscaling or other machine learning-based techniques is out of the scope of this paper.

Trends based on the Mann-Kendall test in offshore wind power densities

In one of the past studies, Gao *et al*.[17] found no significant trend in temperature over the Indian region or northward of 15° – 30° N Lat. Similarly, in this work, no significant trend in GCM-based wind speeds and wind power densities is noticed over the region between 19.8270° N and 21.70° N, as per the Mann-Kendall test[26-28]. However, on a seasonal scale, a decreasing trend in winter is in line with Gao *et al*.[17], and an increasing trend in Gujarat might be attributed to the intensification of monsoon as indicated by Goswami *et al*.[38]. Furthermore, it has been already reported that CMIP6 GCMs predict strengthening of Indian monsoon[39-41].

Seasonal and per-slice wind power densities variation relative to past

In the identified zones in Gujarat, CMIP5 and CMIP6 MME-based results showed an increase in *WPD* in the southwest monsoon (Jun-Sept) rainy season, as shown in Table 3. Further, over the Tamil Nadu zones, CMIP6-based *WPD* increases in winter (Oct-Feb) (Table S2), resulting from the northeast monsoon. Hence, it can be asserted that CMIP6 models suggest strengthening of the monsoon in India as reported by Goswami *et al*.[35] as well as by Jin & Wang[42]. The increase in monsoon is, however, seen lesser in the MME of the CMIP6-based GCMs than CMIP5. This may be attributed to the fact that SSP2-4.5 scenarios of CMIP6 GCMs are associated with more emission of CO_2 than the RCP-4.5 scenarios of CMIP5 GCMs in the considered future slices (2017 to 2050) as shown by Hausfather[43]. In addition, Bollasina *et al*.[44] had remarked that the pollution due to anthropogenic aerosol emission might be weakening the Indian monsoon, hence lesser increase in case of CMIP6 models. Further, both MME-based winds of CMIP5 and CMIP6 GCMs predict a reduction in WPD in future time slices in almost all zones of Gujarat and Tamil Nadu (Table 4). Hence, the secular decrease in wind power potential observed by Gao *et al*.[17] is also observed in this study against Goswami *et al*.'s[35] strengthening of monsoon.

In the summer, CMIP5 MME-based *WPD*s increased relative to past slices in the Gujarat zones, located relatively landwards (Fig. 1a & Table 3). This increase in the summer season for landward regions can be attributed to local geographical and topographical features. As the land heats up faster than the sea in the summer, nearby land regions in Gujarat, such as the Thar desert and the Kathiawar plateau region, heat up, creating a low-pressure zone. It may increase the speed of offshore winds as they blow toward the land. An additional factor in this regard is the tidal drag on the atmosphere amplifying the surface wind[45], especially in the converging channels like the Gulf of Khambhat here as observed by Nayak & Shetye[46] as in summer, tide plays a significant role in that region as reported by Nayak *et al*.[47].

The MME of CMIP6 GCMs, which is closest to the LiDAR location, showed mainly decreasing trends during the summer and winter and an increasing trend during the monsoon season for the Gujarat zones against the findings of Kulkarni *et al*.[15] which earlier predicted that the *WPD* would increase in all the seasons based on MME of CMIP5 GCMs at two offshore locations in Gujarat and Tamil Nadu, namely, Jakhau and Rameswaram. Though CMIP5 and CMIP6-based wind power densities show different trends on a seasonal scale, their time series in each time slice has a statistically significant association as per the Kendall's rank correlation coefficient τ_b (Table 5).

Conclusion

The CMIP6 multi-model ensemble median shows an increase in wind power density during the monsoon season in Gujarat but a decrease in winter. This median better aligns with in-situ observations and CFSR reanalysis than CMIP5 models. However, some individual CMIP5 models perform better with historical CFSR winds and LiDAR data. In Tamil Nadu, CMIP6 models project a decline in wind power density from 2017-2050 for both winter and monsoon, though winter densities remain higher than in the past. The considered downscaling method, that is BIQM with LiDAR-based corrections, yielded results consistent with many past studies in other regions.

Supplementary Data

Supplementary data associated with this article is available in the electronic form at https://nopr.niscpr.res.in/jinfo/ijms/IJMS_53(03)95-108_SupplData.pdf

Acknowledgements

We thank ESGF (Earth System Grid Federation) and acknowledge that CMIP5, CMIP6 and NCEP-CFSR wind data was downloaded from (https://esgf-node.llnl.gov/search/esgf-llnl/). We are grateful to anonymous reviewers for their insightful comments and constructive suggestions.

Conflicts of Interest

Authors declare no conflict of interest.

Author Contributions

ASW & MCD: Conceptualization and formal analysis; ASW: Software and writing- original draft; and MCD: Writing- review & editing and supervision.

References

1 Dash P, Offshore Wind Energy in India, *Akshay Urja*, 12 (2019) 23-25. https://www.researchgate.net/publication/333717700_Offshore_Wind_Energy_in_India

2 Kumar J C R, Kumar D V, Baskar D, Arunsi B M, Jenova R, *et al*., Offshore wind energy status, challenges, opportunities, environmental impacts, occupational health, and safety management in India, *Energy Environ*, 32 (4) (2021) 565-603. https://doi.org/10.1177/0958305X20946483

3 Kamruzzaman M, Shahid S, Islam A T, Hwang S, Cho J, *et al*., Comparison of CMIP6 and CMIP5 model performance in simulating historical precipitation and temperature in Bangladesh: A preliminary study, *Theor Appl Climatol*, 145 (2021) 1385–1406. https://doi.org/10.1007/s00704-021-03691-0

4 Bourdeau-Goulet S-C & Hassanzadeh E, Comparisons between CMIP5 and CMIP6 models: Simulations of climate indices influencing food security, infrastructure resilience, and human health in Canada, *Earth's Future*, 9 (2021) p. e2021EF001995. https://doi.org/10.1029/2021EF001995

5 Li J, Huo R, Chen H, Zhao Y & Zhao T, Comparative Assessment and Future Prediction Using CMIP6 and CMIP5 for Annual Precipitation and Extreme Precipitation Simulation, *Front Earth Sci*, 9 (2021) p. 687976. https://doi.org/10.3389/feart.2021.687976

6 Ministry of New and Renewable Energy, Government of India, *Pre-feasibility Study for Offshore Wind Farm Development in Gujarat*, 2015, pp. 102-103. https://cdnbbsr.s3waas.gov.in/s3716e1b8c6cd17b771da77391355749f3/uploads/2024/12/202412201139752616.pdf

7 Ministry of New and Renewable Energy, Government of India, *Pre-feasibility Study for Offshore Wind Farm Development in Tamil Nadu*, 2015, pp. 104-105. https://cdnbbsr.s3waas.gov.in/s3716e1b8c6cd17b771da77391355749f3/uploads/2022/12/2022121922.pdf

8 FOWIND, Ministry of New and Renewable Energy, Government of India, *Feasibility study for offshore wind farm development in Gujarat*, 2018, pp. 21-153. https://cdnbbsr.s3waas.gov.in/s3716e1b8c6cd17b771da77391355749f3/uploads/2024/12/202412201188073162.pdf

9 FOWIND, Ministry of New and Renewable Energy, Government of India, *Feasibility study for offshore wind farm development in Tamil Nadu*, 2018, pp. 21-149. https://cdnbbsr.s3waas.gov.in/s3716e1b8c6cd17b771da77391355749f3/uploads/2022/12/2022121964.pdf

10 Ministry of New and Renewable Energy, Government of India, *Strategy for establishment of offshore wind energy projects*, 2023, pp. 3-18. https://cdnbbsr.s3waas.gov.in/s3716e1b8c6cd17b771da77391355749f3/uploads/2023/09/20230927103095853 2.pdf

11 Katyal R, *Offshore Wind Energy in India*, NIWE Chennai, Ministry of New and Renewable Energy, Government of India, 2018, pp. 4-26. https://niwe.res.in/assets/Docu/FOWPI/FOWPI-NIWE-Offshore_wind_energy_in_India.pdf

12 Jaswal A K & Koppar A L, Climatology and trends in near-surface wind speed over India during 1961-2008, *MAUSAM*, 64 (3) (2013) 417-436. https://doi.org/10.54302/mausam. v64i3.725

13 Shanas P R & Sanil Kumar V, Temporal variations in the wind and wave climate at a location in the eastern Arabian Sea based on ERA-Interim reanalysis data, *Nat Hazards Earth Syst Sci*, 14 (2014) 1371–1381. https://doi.org/10.5194/nhess-14-1371-2014

14 Kulkarni S, Deo M C & Ghosh S, Comparison of Dynamically and Statistically Downscaled Wind at Selected Indian Offshore Locations, *National Climate Science Conference* (IISc Bangalore), 2015, pp. 93. http://dx.doi.org/10.13140/RG.2.1.2406.5127

15 Kulkarni S, Deo M C & Ghosh S, Framework for Assessment of Climate Change Impact on Offshore Wind Energy, *Met Apps*, 25 (2018) 94-104. https://doi.org/10.1002/met.1673

16 Karnauskas K B, Lundquist J K & Zhang L, Southward shift of the global wind energy resource under high carbon dioxide emissions, *Nature Geosci*, 11 (2018) 38-43. https://doi.org/10.1038/s41561-017-0029-9

17 Gao M, Ding Y, Song S, Lu X, Chen X, *et al*., Secular decrease of wind power potential in India associated with warming in the Indian Ocean, *Sci Adv*, 4 (12) (2018) 1-8. https://doi.org/10.1126/sciadv.aat5256

18 Lakku N K G & Behera M R, Skill and Inter-Model Comparison of Regional and Global Climate Models in Simulating Wind Speed over South Asian Domain, *Climate*, 10 (2022) p. 85. https://doi.org/10.3390/cli10060085

19 Krishnan B, Bastin J, Katyal R & Balaraman K, *Report (First Offshore Lidar Wind Data Analysis)*, National Institute of Wind Energy, Chennai, 2018, pp. 9-10. https://niwe.res.in/assets/Docu/offshore_LiDAR/Dec_2017_to_Nov_2018/6.Report-first_Lidar_Wind_data_analysis.pdf

20 Krishnan B, Bastin J, Katyal R & Balaraman K, *Report (First Offshore Lidar Wind Data (2nd year) Analysis)*, National Institute of Wind Energy, Chennai, 2019, pp. 6-8. https://niwe.res.in/assets/Docu/offshore_LiDAR/Dec_2018_to_Nov_2019/1.Report_on_first_offshore_LiDAR_wind_data (2nd_year)_analysis.pdf

21 Kulkarni S, Deo M C & Ghosh S, Evaluation of wind extremes and wind potential under changing climate for Indian offshore using ensemble of 10 GCMs, *Ocean Coast Manag*, 121 (2016) 141-152. https://doi.org/10.1016/j.ocecoaman.2015.12.008

22 Dragani W C, Martin P B, Simionato C G & Campos M I, Are wind wave heights increasing in south-eastern South American continental shelf between 32°S and 40°S?, *Cont Shelf Res*, 30 (5) (2010) 481-490. https://doi.org/10.1016/j.csr.2010.01.002

23 Li H, Sheffield J & Wood E F, Bias Correction of Monthly Precipitation and Temperature Fields from Intergovernmental Panel on Climate Change AR4 Models Using Equidistant Quantile Matching, *J Geophys Res*, 115 (10) (2010) p. D10101. https://doi.org/10.1029/2009JD012882

24 Al-Buhairi M & Al-Haydari A, Monthly and Seasonal Investigation of Wind Characteristics and Assessment of Wind Energy Potential in Al-Mokha, Yemen, *Energy Power Eng*, 4 (3) (2012) 125-131. http://dx.doi.org/10.4236/epe.2012.43017

25 Akpinar E K & Akpinar S, An Assessment on Seasonal Analysis of Wind Energy Characteristics and Wind Turbine Characteristics, *Energy Convers and Manag*, 46 (11-12) (2005) 1848-1867.

26 Mann H B, Nonparametric tests against the trend, *Econometrica*, 13 (1945) 245-259.

27 Kendall M G, *Rank Correlation Methods*, 4th edn, (Griffin, London), 1975, pp. 210.

28 Fatichi S, *Mann-Kendall Test*, MATLAB Central File Exchange, https://www.mathworks.com/matlabcentral/fileexchange/25531-mann-kendall-test; version (03/2024).

29 Krishnan A & Bhaskaran P K, Skill assessment of global climate model wind speed from CMIP5 and CMIP6 and evaluation of projections for the Bay of Bengal, *Clim Dyn*, 55 (9) (2020) 2667-2687. https://doi.org/10.1007/s00382-020-05406-z

30 Saha S, Moorthi S, Pan H, Wu X, Wang J, *et al*., The NCEP Climate Forecast System Reanalysis, *Bull Amer Meteor Soc*, 91 (8) (2010) 1015-1058. https://doi.org/10.1175/2010BAMS3001.1

31 Saha S, Moorthi S, Wu X, Wang J, Nadiga S, *et al*., The NCEP Climate Forecast System Version 2, *J Climate*, 27 (6) (2014) 2185-2208. https://doi.org/10.1175/JCLI-D-12-00823.1

32 Sajidh C K & Chatterjee A, Indian Ocean dynamic sea level, its variability and projections in CMIP6 models, *Clim Dyn*, 61 (2023) 2229–2252. https://doi.org/10.1007/s00382-023-06676-z

33 Hagemann S, Chen C, Haerter J O, Heinke J, Gerten D, *et al*., Impact of a Statistical Bias Correction on the Projected Hydrological Changes Obtained from Three GCMs and Two Hydrology Models, *J Hydrometeor*, 12 (4) (2011) 556-578. https://doi.org/10.1175/2011JHM1336.1

34 Themeßl M J, Gobiet A & Heinrich G, Empirical-statistical downscaling and error correction of regional climate models and its impact on the climate change signal, *Clim Change*, 112 (2012) 449-468. https://doi.org/10.1007/s10584-011-0224-4

35 Maraun D, Bias Correction, Quantile Mapping, and Downscaling: Revisiting the Inflation Issue, *J Climate*, 26 (6) (2013) 2137-2143. https://doi.org/10.1175/JCLI-D-12-00821.1

36 Maurer E P & Pierce D W, Bias correction can modify climate model simulated precipitation changes without adverse effect on the ensemble mean, *Hydrol Earth Syst Sci*, 18 (2014) 915-925. https://doi.org/10.5194/hess-18-915-2014

37 Cannon A J, Sobie S R & Murdock T Q, Bias Correction of GCM Precipitation by Quantile Mapping: How Well Do Methods Preserve Changes in Quantiles and Extremes?, *J Climate*, 28 (17) (2015) 6938-6959. https://doi.org/10.1175/JCLI-D-14-00754.1

38 Goswami B N, Venugopal V, Sengupta D, Madhusoodanan M S & Xavier P K, Increasing Trend of Extreme Rain Events Over India in Warming Environment, *Science*, 314 (2006) 1442-1445. https://www.science.org/doi/10.1126/science.1132027

39 Katzenberger A, Schewe J, Pongratz J & Levermann A, Robust increase of Indian monsoon rainfall and its variability under future warming in CMIP6 models, *Earth Syst Dynam*, 12 (2021) 367–386, https://doi.org/10.5194/esd-12-367-2021.

40 Katzenberger A, Levermann A, Schewe J & Pongratz J, Intensification of very wet monsoon seasons in India under global warming, *Geophys Res Lett*, 49 (2022) p. e2022GL098856, https://doi.org/10.1029/2022GL098856

41 Joseph L, Skliris N, Dey D, Marsh R & Hirschi J, Increased summer monsoon rainfall over Northwest India caused by Hadley cell expansion and Indian Ocean warming, *Geophys Res Lett*, 51 (2024) p. e2024GL108829. https://doi.org/10.1029/2024GL108829

42 Jin Q & Wang C, A revival of Indian summer monsoon rainfall since 2002, *Nature Clim Change*, 7 (2017) 587-594. https://doi.org/10.1038/nclimate3348

43 Hausfather Z, CMIP6: The next generation of climate models explained, *Carbon Brief*, https://www.carbonbrief.org/cmip6-the-next-generation-of-climate-models-explained/ (06/2022)

44 Bollasina M A, Ming Y & Ramaswamy V, Anthropogenic aerosols and the Weakening of the South Asian Summer Monsoon, *Science*, 334 (2011) 502-505. https://doi.org/10.1126/science.1204994

45 Renault L & Marchesiello P, Ocean tides can drag the atmosphere and cause tidal winds over broad continental shelves, *Commun Earth Environ*, 3 (2022) 1-7. https://doi.org/10.1038/s43247-022-00403-y

46 Nayak R K & Shete S R, Tides in the Gulf of Khambhat, west coast of India, *Estuar Coast Shelf Sci*, 57 (1-2) (2003) 249-254. https://doi.org/10.1016/S0272-7714(02)00349-9

47 Nayak R K, Salim M, Mitra D, Sridhar P N, Mohanty P C, *et al*., Tidal and Residual Circulation in the Gulf of Khambhat and its Surrounding on the West Coast of India, *J Indian Soc Remote Sens*, 43 (2015) 151-162. https://doi.org/10.1007/s12524-014-0387-3